Spectroscopic factors in ^{40}Ca and ^{208}Pb from $(e, e'p)$: Fully relativistic analysis

J. M. Udías, P. Sarriguren, E. Moya de Guerra, E. Garrido, and J. A. Caballero
Instituto de Estructura de la Materia, Consejo Superior de Investigaciones Científicas, Serrano 119, E-28006 Madrid, Spain
(Received 3 June 1993)

We present results for spectroscopic factors of the outermost shells in ^{40}Ca and ^{208}Pb, which have been derived from the comparison between the available quasielastic $(e, e'p)$ data from NIKHEF-K and the corresponding calculated cross sections obtained within a fully relativistic formalism. We include exactly the effect of Coulomb distortion on the electron wave functions and discuss its role in the extraction of the spectroscopic factors from experiment. Without any adjustable parameter, we find spectroscopic factors of about 70%, consistent with theoretical predictions. We compare our results with previous relativistic and nonrelativistic analyses of $(e, e'p)$ data. In addition to Coulomb distortion effects, we discuss different choices of the nucleon current operator and also analyze the effects due to the relativistic treatment of the outgoing-distorted and bound nucleon wave functions.

PACS number(s): 25.30.Fj, 24.10.Jv, 21.10.Jx

I. INTRODUCTION

Spectroscopic factors and occupation probabilities are basic elements for our understanding of the nuclear structure, measuring the accuracy of the shell model description. The fundamental concept on which the shell model is based, the mean field approximation, is considered as the leading contribution in an expansion of multiparticle correlations within the general framework of the nuclear many-body theory. These correlations allow the nucleons to occupy partially different orbits above and below the Fermi level. Therefore, the deviation from full occupancy of the orbits below the Fermi level is a measure of the correlations neglected in the mean field approach, or in other words, a check of the validity of the mean field description.

The spectroscopic factor S_α is defined as the probability to reach a final single-particle (hole) state α when a nucleon is added to (removed from) the target nucleus. The occupation number N_α is the number of nucleons in the quantum state α in the target nucleus, relative to the $2j + 1$ limit.

Theoretical spectroscopic factors and occupation numbers have been derived for some doubly magic nuclei, taking into account both short- and long-range correlations. In particular, occupation numbers for the $3s_{1/2}$ state in ^{208}Pb have been obtained from different approaches. Mahaux and Sartor [1] derived an occupation number $N_{3s} = 0.83$ and a spectroscopic factor $S_{3s} = 0.69$ by using a dispersion relation approach, which allows one to extrapolate the empirical mean field from positive energies (optical potential) to negative energies (shell model potential). Slightly smaller spectroscopic factors have been obtained by Ma and Wambach [2] using a quasiparticle Hamiltonian which includes correlations in a phenomenological way. Pandharipande and collaborators [3] obtained an average value 0.71 ± 0.1 for the occupation probabilities of single-particle states just below the Fermi level, using a variational calculation of nuclear matter to which a random phase approximation correction is added.

From the experimental point of view, relative spectroscopic factors have been historically determined by single-nucleon transfer reactions. In a search for absolute empirical values of spectroscopic factors, additional experimental information has been recently collected from two new sources. One is based on a sum-rule analysis [4] of both transfer data and charge density differences of isotones extracted from (e, e') reactions. This method allows going from relative spectroscopic factors to an absolute occupation number (see Ref. [5] and references therein). A typical value for the occupation number of the $3s_{1/2}$ shell in ^{208}Pb obtained from this method is $N_{3s} = 0.78 \pm 0.12$ [5].

The other method is the quasielastic $(e, e'p)$ reaction, which constitutes indeed a very well suited tool to extract experimental information on absolute spectroscopic factors. Modern facilities allow studying this reaction in detail and high precision measurements of cross sections are available [6–8]. The small strength of the electromagnetic interaction allows one to study the transition in Born approximation (BA) by the exchange of a single virtual photon. Choosing properly the momentum and energy transferred by the virtual photon in order to satisfy the quasielastic condition ($\omega \simeq q^2/2M$), the process can be treated with confidence [9] in impulse approximation (IA), i.e., assuming that the exchanged photon is absorbed by a single nucleon which is the one detected. Under these circumstances, it is possible to extract information on the energy and momentum distribution of the bound nucleon.

Although the advantages of the $(e, e'p)$ process over other possible reactions to study spectroscopic factors are widely recognized, the extraction of these factors from experiment is still not free of ambiguities. A reliable determination of spectroscopic factors requires an accurate knowledge of the mechanism of the reaction and, in this context, the exact treatment of the Coulomb distortion

of the electrons is important, especially in heavy nuclei such as lead.

Different methods have been proposed to handle the distortion. The early approaches were based on the eikonal approximation [10] within a nonrelativistic scenario for the nuclear part. This method was applied to the analysis of $(e,e'p)$ data taken at NIKHEF-K [6,7], producing surprisingly low spectroscopic factors (0.49 ± 0.05 for the $3s_{1/2}$ shell in ^{208}Pb), incompatible with results obtained from other reactions as well as with theoretical predictions. This fact, together with the large difference between the results from first and second order eikonal calculations, raised the question of whether this approximation was adequate to treat the Coulomb distortion or a more involved analysis was still needed.

The first realistic calculations with a more exact treatment of the Coulomb distortion in $(e,e'p)$ were made in 1990 by McDermott [11]. The incorporation of the distortion effects was achieved by means of a full partial wave analysis of the electron waves in the Coulomb potential of the target, as well as of the outgoing proton waves distorted by the optical potential. The complexity of the numerical calculations required a full relativistic framework, not only for the electron vertex where the energies involved in the experiments (hundreds of MeV) make it mandatory, but also for the nuclear vertex. Nevertheless, some approximations were still made (helicity conserved approximation, HCA) to simplify the treatment of the electron Coulomb distorted waves. The spectroscopic factor for the $3s_{1/2}$ shell in ^{208}Pb amounts in this approximation to 0.65 [11], manifestly above the value obtained within the eikonal approximation.

Subsequently, a new relativistic calculation was reported by Jin *et al.* [12], where the treatment of the Coulomb distortion of the electrons was exact and the above-mentioned restricted approximation (HCA) was not made. The result of this calculation [12] for the spectroscopic factor in the same shell is 0.71, which is larger than the result of Ref. [11]. The authors of Ref. [12] reported also some discrepancies with the results of Ref. [11] in the limit of plane waves for the electron (no Coulomb distortion) and stressed the need for further investigation.

This paper is an attempt to clarify this situation by an independent analysis including the development of a new code [13], which treats the Coulomb distortion of the electron in an exact way and uses a relativistic formalism for both the leptonic and the nuclear vertices. Our calculations are along similar lines to those of Ref. [12], though in some instances we use a different nucleon current operator and different bound nucleon wave functions. Differences and similarities with previous calculations in Refs. [11,12] are discussed in detail in the next sections, which are organized as follows: In Sec. II we summarize briefly the formalism involved in our calculations. In Sec. III we discuss our results for the $3s_{1/2}$ and $2d_{3/2}$ shells in ^{208}Pb and for the $2s_{1/2}$ and $1d_{3/2}$ shells in ^{40}Ca. We discuss not only the effect of Coulomb distortion but also the effect of the relativistic optical potential and of nucleon current operator. Section IV summarizes the main conclusions.

II. DESCRIPTION OF CALCULATIONS

In this section we summarize the formalism used to describe the coincidence $(e,e'p)$ reaction under the conditions defining the IA discussed in the Introduction. Figure 1 represents graphically the $(e,e'p)$ process. In this figure k_i^μ (k_f^μ) is the four-momentum of the incoming (outgoing) electron and q^μ is the four-momentum of the exchanged photon. The ejected proton four-momentum is denoted by P_F^μ. We use the notation and conventions of Ref. [14] as well as $\hbar = c = 1$. As represented in Fig. 1 the electromagnetic transition is treated in Born approximation, although we take into account the effect of the nuclear Coulomb potential to all orders by using electron distorted wave functions.

The differential cross section for this process is then written as [13]

$$\frac{d^4\sigma}{d\epsilon_f d\Omega_f dE_F d\Omega_F} = \frac{\delta(\epsilon_i + E_A - \epsilon_f - E_F - E_{A-1})}{(2\pi)^5} \times 4\alpha^2 \epsilon_f^2 E_F |\mathbf{P}_F| \overline{\sum} |W_{if}|^2 , \quad (2.1)$$

where $\overline{\Sigma}$ indicates sum (average) over final (initial) polarizations and

$$W_{if} = \int d\mathbf{x} \int d\mathbf{y} \int \frac{d\mathbf{q}}{(2\pi)^2} j_\mu^e(\mathbf{x}) e^{-i\mathbf{q}\cdot(\mathbf{x}-\mathbf{y})} \frac{(-1)}{q_\mu^2} J_N^\mu(\mathbf{y}) . \quad (2.2)$$

In this expression j_μ^e and J_N^μ stand for the electron and nuclear currents, respectively. The electron current is given by the well-known pointlike Dirac particle expression:

$$j_e^\mu(\mathbf{r}) = \bar{\psi}_f^e(\mathbf{r}) \gamma^\mu \psi_i^e(\mathbf{r}) , \quad (2.3)$$

where ψ_i^e, ψ_f^e stand for initial and final electron wave functions. In IA and within an independent particle model picture, the nuclear current can be written in terms of the nucleon current operator $\hat{J}_N^\mu$:

$$J_N^\mu(\mathbf{r}) = \bar{\psi}_F^N(\mathbf{r}) \hat{J}_N^\mu \psi_B^N(\mathbf{r}) , \quad (2.4)$$

with ψ_B^N, ψ_F^N the wave functions for the initial bound nucleon and final nucleon, respectively, and $\hat{J}_N^\mu$ a nucleon current operator to be specified later.

The initial and final electron wave functions, solutions of the Dirac equation with the Coulomb potential, have the form

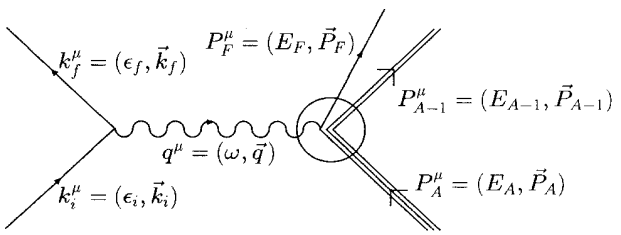

FIG. 1. Schematic picture of the $(e,e'p)$ process.

$$\psi_i^e(\mathbf{r}) = 4\pi\sqrt{\frac{\epsilon_i+m}{2\epsilon_i}}\sum_{\kappa,\mu,m} e^{i\delta_\kappa} i^l \langle l\ m\ \tfrac{1}{2}\ \sigma_i | j\ \mu\rangle \times Y^*_{lm}(\hat{k}_i)\psi^\mu_\kappa(\mathbf{r})\ , \quad (2.5)$$

where the functions

$$\psi^\mu_\kappa(\mathbf{r}) = \begin{pmatrix} g_\kappa(r)\phi^\mu_\kappa(\hat{r}) \\ i f_\kappa(r)\phi^\mu_{-\kappa}(\hat{r}) \end{pmatrix} \quad (2.6)$$

are eigenstates of total angular momentum with quantum numbers $\kappa\mu$ ($j = |\kappa| - 1/2$; $l = \kappa$ if $\kappa > 0$ and $l = -\kappa - 1$ if $\kappa < 0$). The functions f_κ, g_κ satisfy the usual radial equations [15] and $\phi^\mu_\kappa(\hat{r})$ is given by

$$\phi^\mu_\kappa(\hat{r}) = [Y_l \otimes \boldsymbol{\sigma}]^\mu_j \equiv \sum_{m,\sigma}\langle l\ m\ \tfrac{1}{2}\ \sigma |\ j\ \mu\rangle Y_{lm}(\hat{r})\chi^{\frac{1}{2}}_\sigma\ . \quad (2.7)$$

For the outgoing electron wave function ψ^e_f, the phase shifts δ_κ have to be included with a minus sign. The functions f_κ, g_κ and the phase shifts are obtained by numerical integration of the radial equations using the Milne procedure, as described in the work of Yennie *et al.* [16], including up to third derivatives. The Coulomb potentials for ^{208}Pb and ^{40}Ca are derived from the experimental charge distributions given in Ref. [17].

The bound-state wave functions for the proton ψ^N_B are spinors with well-defined angular momentum quantum numbers $\kappa_B\mu_B$, and have a structure similar to that in Eq. (2.6). They have been computed within the framework of the relativistic independent particle shell model. The mean field in the Dirac equation is determined through a Hartree procedure from a phenomenological relativistic Lagrangian with scalar and vector S-V terms. We use the parameters of Ref. [18], which are fitted to reproduce nuclear matter properties and the charge radius in ^{40}Ca, and the TIMORA code [19].

The wave function of the detected proton ψ^N_F is a scattering solution of a Dirac-like equation, which includes S-V global optical potentials, obtained by fitting elastic proton scattering data [20]. This wave function has basically the same structure of Eq. (2.5) except that, since the potential is in this case complex, the phase shifts and radial functions are also complex. In addition, since the wave function corresponds to an outgoing proton we have to use in Eq. (2.6) the complex conjugates $f^\star_\kappa, g^\star_\kappa$ and in Eq. (2.5) the complex conjugate $\delta^\star$ with a negative sign.

For the current operator we consider the two choices $cc1$ and $cc2$ introduced by de Forest [21] in momentum space:

$$\hat{J}^\mu_N(cc1) = (F_1 + \bar{\kappa}F_2)\gamma^\mu - \frac{\bar{\kappa}F_2}{2M}(P_F + \bar{P}_I)^\mu\ , \quad (2.8)$$

$$\hat{J}^\mu_N(cc2) = F_1\gamma^\mu + i\frac{\bar{\kappa}F_2}{2M}\sigma^{\mu\nu}q_\nu\ , \quad (2.9)$$

where F_1 and F_2 are the nucleon form factors related in the usual way [14] to the electric and magnetic Sachs form factors of the dipole form. $\bar{P}_I$ in Eq. (2.8) is the four-momentum of the initial nucleon assuming on-shell kinematics [21].

As it is well known [14], Eqs. (2.8) and (2.9) are equivalent when the initial and final nucleons are on-shell. For off-shell nucleons, as is our case, both expressions lead to different results and do not satisfy current conservation. In configuration space all three-momenta in Eqs. (2.8) and (2.9) have to be considered as operators. For the $cc2$ choice, integration by parts allows one to replace the gradient operators acting on ψ^N_B, ψ^N_F by $\mathbf{q}$, the variable of integration in Eq. (2.2). In the case of the $cc1$ choice, it is not possible to get rid of the gradient operator acting on at least one of the nucleon wave functions. Given the fact that for off-shell nucleons none of the expressions $(cc1, cc2)$ is fully satisfactory and both expressions fail to verify current conservation, when using the choice $cc1$ we use the simplifying assumption of replacing $\hat{\mathbf{P}}_F + \hat{\mathbf{P}}_I$ by the asymptotic $\mathbf{P}_F + \mathbf{P}_m$ values, with $\mathbf{P}_m$ the missing momentum. This assumption simplifies enormously the calculations and is consistent with the prescription of de Forest in Ref. [21] for the half-off-shell electron-proton cross section $\sigma(cc1)$, which is commonly used. In the same spirit F_1 and F_2 are taken as the standard nucleon form factors at the asymptotic q values, an approximation usually made when Coulomb distorted electron waves are employed [11,12]. Under this approximation the computation time is highly reduced.

The operator $cc2$ was used in previous fully relativistic calculations [11,12]. In this work we use both $cc1$ and $cc2$ operators. Comparisons between half-off-shell electron-proton cross sections obtained with both operators ($cc1$ and $cc2$) have previously been made using plane waves for initial and final nucleons [21,22]. In Refs. [21,22] small differences (a few percent) were found at the kinematical conditions usually attained in the experiments. In the next section we present similar comparisons when realistic spinors are used to obtain the cross section.

Different notations have been introduced in the literature by different authors to distinguish various degrees of approximations to the reaction mechanism. To avoid confusion we shall specify separately the approximation taken at each vertex, i.e., at the electronic and at the nuclear vertices. To distinguish the case when we use plane waves from the case when we use distorted waves in the electron current [Eq. (2.3)], we use the notations PWBA and DWBA, respectively. On the other hand, to distinguish the cases when we use plane waves and distorted waves for the ejected proton, we use the notation PWIA and DWIA, respectively. Unless otherwise specified, the results presented are obtained with proton distorted waves (DWIA). In PWBA the electron current is given by

$$j^\mu_{e,\text{free}}(\mathbf{r}) = \frac{m}{\sqrt{\epsilon_i\epsilon_f}}e^{i(\mathbf{k}_i-\mathbf{k}_f)\cdot\mathbf{r}}\bar{u}(\mathbf{k}_f,\sigma_f)\gamma^\mu u(\mathbf{k}_i,\sigma_i)\ . \quad (2.10)$$

In the same way, when the optical potential is not included in the calculations (PWIA), the wave function of the ejected proton ψ^N_F becomes a plane wave in the corresponding equation for the nuclear current.

A few remarks concerning the numerical calculations in DWBA are in order. The truncation of the infinite sum over κ in Eq. (2.5) has been made to include at least 30 partial waves for both initial and final electrons, as well

as for the outgoing proton in DWIA. The radial integrals in Eq. (2.2) have been carried out numerically up to typically 15 fm in the nuclear coordinate and 30 fm in the electron coordinate. This gives a good compromise in optimizing both numerical accuracy and computing time. The numerical accuracy has been checked by comparison to PWBA of the results obtained in DWBA for $Z \to 0$. The estimated numerical error amounts to less than 2% in the spectroscopic factors [13].

III. RESULTS

We present our results in terms of reduced cross sections $\rho(P_m)$ for selected E_m values (i.e., for selected single-particle shells), defined by

$$\rho(P_m) = \int_{\Delta E_m} dE_m \ [\sigma_{ep}|\mathbf{P}_F|E_F]^{-1} \frac{d^4\sigma}{dE_F d\epsilon_f d\Omega_F d\Omega_f} , \tag{3.1}$$

as functions of the missing momentum ($\mathbf{P}_m = \mathbf{P}_A - \mathbf{P}_{A-1}$). Experimentally, the integral over the missing energy ($E_m = M_{A-1} + M - M_A$) is taken over the interval ΔE_m that contains the peak of the transition under study. In our calculations of $\rho(P_m)$, we take for σ_{ep} in Eq. (3.1) the same expression used by the experimentalists, i.e., we use the expression σ_{cc1} given by Eq. (17) of Ref. [21].

We present results for the $3s_{1/2}$ and $2d_{3/2}$ shells in ^{208}Pb and for the $2s_{1/2}$ and $1d_{3/2}$ shells in ^{40}Ca and compare with data in parallel kinematics ($\mathbf{q} \parallel \mathbf{P}_F$). We have chosen to study these shells for several reasons: (i) they correspond to experimentally well-separated peaks, (ii) for these doubly magic nuclei the theoretical description is simpler and there are available optical potentials, (iii) this choice allows us to study different mass regions where the Coulomb distortion of the electron waves is expected to play a different role, and (iv) for these shells we can compare our results with experimental data as well as with other relativistic and/or nonrelativistic theoretical results. Unless otherwise specified the results presented correspond to parallel kinematics ($\mathbf{q} \parallel \mathbf{P}_F$). All the calculations have been done for a fixed value of the kinetic energy of the outgoing proton ($T_F = 100$ MeV). We also take a fixed value of the incoming electron energy, $\epsilon_i = 412$ MeV (375 MeV) for ^{208}Pb (^{40}Ca).

A. $3s_{1/2}$ shell of ^{208}Pb

We discuss results on the $3s_{1/2}$ shell in detail because this shell is the most extensively studied in $(e, e'p)$, both experimentally and theoretically.

To start with, it is worth clarifying the situation with regard to the disagreement between the PWBA results in Refs. [11,12]. As pointed out in Ref. [12], both calculations being the same in PWBA should lead to the same results. We found that the reason for the disagreement is due to the fact that different wave functions were used for the bound proton. In our calculations we used the code by Horowitz and Serot (TIMORA) with the standard set of initial conditions and obtained a result [see dashed line in Fig. 2(a)] in agreement with that in Ref. [12]. With the same code but changing the initial conditions to those used by McDermott [11,23], we find a result [see dotted line in Fig. 2(a)] that agrees with the result in Ref. [11]. As indicated in the figure, the two above-mentioned results have been obtained with the operator $cc2$, which is the operator always used in Refs. [11,12].

In what follows we use always for the bound proton the wave function obtained with the standard set of initial conditions. This wave function corresponds to a binding energy of 5.7 MeV.

In Fig. 2(a) we also show our result (solid line) in PWBA corresponding to the choice $cc1$ for the current operator. As seen in this figure the PWBA results obtained with $cc1$ (solid) and $cc2$ (dashed) current operators are very close. The main difference seen at the peaks is less than 8%, the $cc1$ result being larger.

In Fig. 2(b) we show our DWBA results obtained with the $cc1$ operator (solid line) together with the DWBA results of Ref. [12] (dashed line) that was obtained with the $cc2$ operator. Also shown in this figure is the result obtained with the code of McDermott, used in Ref. [11], that makes use of the HCA (dotted line). In this figure, the three curves are obtained using the same relativistic optical potential [20] and also the same wave function for the bound proton. One can see that our results (solid line) and those from Ref. [12] (dashed line) are similar and show up the same qualitative changes with respect to the corresponding PWBA results shown in Fig. 2(a). These changes are (i) a shift in P_m, (ii) an increase at the maxima, and (iii) a filling of the minimum at $P_m \sim 150$ MeV. Note that the result obtained within HCA [dotted line in Fig. 2(b)] is not able to reproduce the two last mentioned effects (focusing effects) but it reproduces adequately the shift in P_m.

In Fig. 3(a) we show in more detail the comparison between our PWBA and DWBA results shown by the dotted and solid lines, respectively. Also shown in Fig. 3(a) is the PWBA result with an effective q value (dashed line), $q_{\text{eff}} = |\mathbf{k}_{i,\text{eff}} - \mathbf{k}_{f,\text{eff}}|$, where the electron initial and

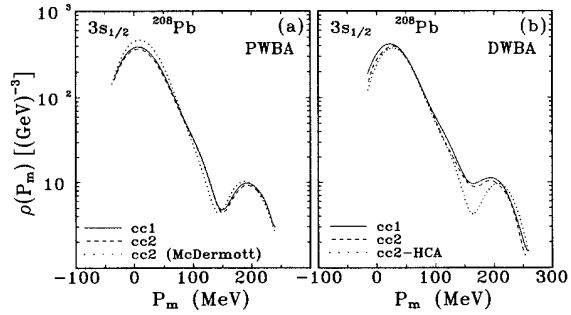

FIG. 2. Reduced cross sections for the shell $3s_{1/2}$ of ^{208}Pb in DWIA. (a) Comparison of PWBA results with the $cc1$ and $cc2$ operators. The dashed and dotted lines correspond to different choices of the $3s_{1/2}$ wave function. (b) Comparison of DWBA results with $cc1$ and $cc2$ operators. See text.

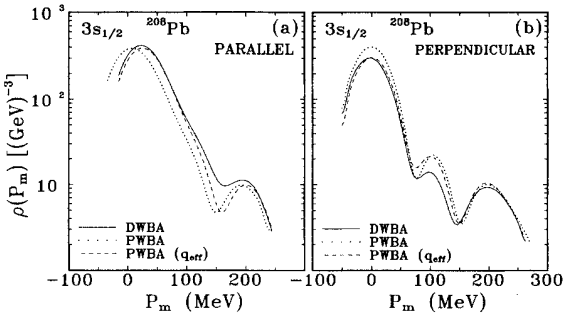

FIG. 3. Reduced cross sections for the shell $3s_{1/2}$ of ^{208}Pb in DWIA corresponding to parallel (a) and perpendicular (b) kinematics. The results obtained in DWBA are compared to the results in PWBA with and without effective momentum transfer.

final effective momenta are given by

$$\mathbf{k}_{\rm eff} = \mathbf{k} + f_c \frac{Z\alpha}{R} \frac{\mathbf{k}}{|\mathbf{k}|} \tag{3.2}$$

with $R = 1.1\ A^{1/3}$ fm and $f_c = 1.35$. This f_c value has been adjusted to get the same Coulomb potential at the origin that corresponds to the charge distribution of the nuclear target obtained from the relativistic calculation, which agrees with the experimental one [17]. This value is somewhat smaller than the value $f_c = 3/2$, corresponding to a spherical uniform charge distribution. In parallel kinematics, since $P_m = q - P_F$ is varied by varying q, a displacement in q produces a displacement in P_m. As seen in Fig. 3(a), with this f_c value the shift in P_m caused by electron Coulomb distortion is well accounted for.

It should be pointed out that the effect of Coulomb distortion shows up differently in perpendicular kinematics (constant q and ω). To illustrate this point we show in Fig. 3(b) the comparison between our results in PWBA and DWBA in perpendicular kinematics. In this case there is no observable effect of displacement with P_m but there is a reduction of the cross section in DWBA at $P_m \sim 0$ that, as seen in the figure, is accounted for replacing q by $q_{\rm eff}$ in PWBA. The reduction is due to the fact that the maximum of the bound nucleon wave function (s wave) at $P_m = 0$ is not reached when q is replaced by $q_{\rm eff}$. The actual effect of the focusing is of the same order in perpendicular kinematics as in parallel kinematics. On the other hand, changing q into $q_{\rm eff}$ produces quite a different effect in perpendicular kinematics because in this case P_m is varied keeping q constant and varying the angle between $\mathbf{q}$ and $\mathbf{P}_F$. In what follows only the case of parallel kinematics is considered.

The focusing effects, causing the filling of the minimum and increase of the maxima in Fig. 3(a), are summarized in a quantitative way in Table I. In this table we quote the ratios between the reduced cross sections calculated in DWBA and in PWBA at the two maxima. We compare the ratios obtained in this work with the ratios deduced from other relativistic and nonrelativistic calculations previously reported. The nonrelativistic results in Table I correspond to the code DWEEPY [10]. This code treats the Coulomb distortion in an approximate way making use of an expansion in powers of $(Z\alpha/k)$ to first order (DWEEPY1) or to second order (DWEEPY2). DWEEPY2 is the most commonly used approximation in the nonrelativistic analyses of the data. One can see in Table I that our results and those of Ref. [12], which also treat Coulomb distortion in an exact way, are in very good agreement. The results obtained with the HCA code of McDermott [11,23] do not reproduce adequately the focusing effect at the peaks. Among the nonrelativistic calculations, DWEEPY1 overestimates largely the effect of focusing and DWEEPY2 gives still an overestimation. The spectroscopic factors are very sensitive to focusing effects because these factors are derived by scaling the theoretical reduced cross section to the experimental one. As seen in Table I the various approaches to treat the electron Coulomb distortion fail to account for the focusing effect obtained with the exact DWBA calculation, which is non-negligible in ^{208}Pb. Therefore, DWBA calculations are necessary to deduce reliable spectroscopic factors in heavy nuclei such as lead.

In comparing relativistic and nonrelativistic calculations, it is also important to know how different approximations for the proton wave functions affect the reduced cross section. To this end we compare in Fig. 4 the results of relativistic and nonrelativistic calculations in PWBA because in this case there is no effect from electron Coulomb distortion and the differences come only from the various approximations at the nuclear vertex.

In Fig. 4 the dotted and dashed lines show the PWIA results of the relativistic and nonrelativistic calculations, respectively. The solid and short-dashed lines show the results in DWIA of relativistic and nonrelativistic calculations. For the relativistic calculations we use the nuclear current operator J_{cc2} in Eq. (2.9) and the standard TIMORA solution [19] for the relativistic bound proton wave function. For the nonrelativistic bound proton wave function we use the upper component of the relativistic one, properly normalized, in the standard nonrelativistic form of the nucleon current, based on $cc2$ [24]. The nonrelativistic optical potential has been taken from set II in Table 2.1 of Ref. [6], which was determined following the procedure of Ref. [25]. This set gives a good fit to

TABLE I. Ratio between DWBA and PWBA reduced cross sections at the two maxima in the $3s_{1/2}$ shell of ^{208}Pb ($T_F = 100$ MeV and $\epsilon_i = 412$ MeV with parallel kinematics).

	This work	Jin *et al.* [12]	HCA	DWEEPY1[a]	DWEEPY2[a]
First maximum	1.08	1.08	0.98	1.92	1.21
Second maximum	1.14	1.13	1.03	–	–

[a]Extracted from Ref. [10].

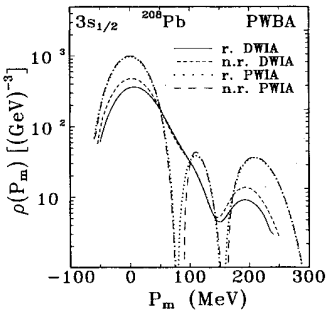

FIG. 4. Comparison of PWBA results from relativistic (r.) and nonrelativistic (n.r.) calculations in DWIA and PWIA for the $3s_{1/2}$ shell in ^{208}Pb.

elastic proton scattering data [26] from ^{208}Pb at an energy of 98 MeV (which roughly corresponds to the proton energy involved in the $(e,e'p)$ experiments [6]). On the other hand, the relativistic optical potential used here was determined [20] from a global fit to elastic proton scattering data from spherical nuclei with mass numbers $40 \leq A \leq 208$ in a wide range of projectile energies from 65 MeV to 1040 MeV.

As seen in Fig. 4, both relativistic and nonrelativistic calculations give practically the same result in PWIA. The same is true when a Woods-Saxon potential is used for the bound nucleon [13]. This means that the use of nonrelativistic bound nucleon wave functions does not produce a significant change in the P_m range considered.

The differences between relativistic and nonrelativistic calculations are much more noticeable in DWIA. As seen in Fig. 4, the shape is similar in both DWIA calculations but the relativistic potential leads to stronger absorption than the nonrelativistic one (about a 20% difference at the peaks). This is at first sight surprising since both potentials reproduce well the elastic scattering of protons from this nucleus at proton energies of about 100 MeV. Therefore, the difference seen between the DWIA results in Fig. 4 must be attributed to details of the optical potential to which the elastic proton scattering at this energy is not sensitive.

As it is well known [18] the relativistic S-V potential gives rise to nonlocal terms in the nonrelativistic reduction. The effect of these terms in the $(e,e'p)$ reaction was investigated by Boffi and collaborators [27]. The authors of Ref. [27] concluded that these terms only affect the inelastic processes, where the nuclear interior is important, producing about a 15% increase of the absorption due to final-state interactions in the $(e,e'p)$ reaction. This conclusion is in agreement with the increased absorption observed in Fig. 4 in going from the nonrelativistic DWIA to the relativistic DWIA. It would be interesting to see to what extent the nonrelativistic reduction of the S-V optical potential [20] may lead to a similar absorption as the relativistic DWIA. Work along these lines is in progress.

B. Comparison with experiment

The main results of this work are presented in Table II and in Fig. 5, where we compare our relativistic DWBA results to the experimental data, in parallel kinematics. Our theoretical results are given by the solid lines in Fig. 5 and have been scaled by the spectroscopic factors presented in Table II.

Our spectroscopic factors for the $3s_{1/2}$ and $2d_{3/2}$ shells in ^{208}Pb, and for the $2s_{1/2}$ and $1d_{3/2}$ shells in ^{40}Ca, are given in the third and fourth columns of Table II, corresponding to calculations with *cc*1 and *cc*2 operators, respectively. They have been obtained by scaling our theoretical results on $\rho(P_m)$ to the experimental data from Refs. [6,7] shown in Fig. 5. For each shell the overall scale factor (spectroscopic factor) has been obtained by means of an error weighted least-squares procedure. The quoted errors in our spectroscopic factors include both statistical and systematical errors in experimental data [6,7]. Also given for comparison in Table II are the spectroscopic factors obtained from other relativistic and nonrelativistic calculations. The spectroscopic factors reported by Jin *et al.* [12] have been obtained with a fully relativistic DWBA formalism similar to the one used in this work, using the *cc*2 current operator. As discussed in the previous section, in the case of the $3s_{1/2}$ shell in ^{208}Pb the authors of Ref. [12] use the same bound nucleon wave function used here. For ^{40}Ca the bound nucleon wave functions used in Ref. [12] are different [28] from the standard TIMORA solutions used here. In column six of Table II we quote the spectroscopic factors obtained by McDermott [11] using also the *cc*2 operator. The last column of Table II contains the spectroscopic factors obtained with the nonrelativistic analyses reported in Refs. [6,7].

As seen in Table II, in general, the spectroscopic factors obtained with the *cc*2 current operator are somewhat larger than those obtained with *cc*1. For ^{208}Pb our *cc*2 results differ by less than 10% from the *cc*1 results and are in agreement with the corresponding result by Jin *et al.* [12]. As discussed in the previous section, the result by McDermott [11] does not contain the correct focus-

TABLE II. Comparison of our spectroscopic factors obtained with the *cc*1 and *cc*2 operators and with other relativistic and nonrelativistic analyses.

		cc1	cc2	Jin *et al.* [12]	McDermott [11]	Nonrel.
^{208}Pb	$3s_{1/2}$	0.65(4)	0.70(4)	0.71	0.65	0.50(5)[a]
	$2d_{3/2}$	0.66(4)	0.73(4)	–	–	0.53(4)[a]
^{40}Ca	$2s_{1/2}$	0.44(3)	0.51(3)	0.75	–	0.50(6)[b]
	$1d_{3/2}$	0.60(3)	0.76(4)	0.80	0.66	0.65(5)[b]

[a]From Ref. [6].
[b]From Ref. [7].

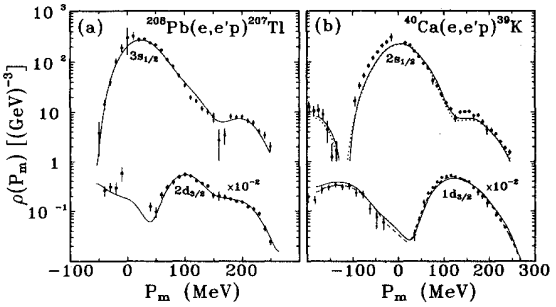

FIG. 5. Theoretical and experimental reduced cross sections for the $3s_{1/2}$ and $2d_{3/2}$ shells in ^{208}Pb (a) and for the $2s_{1/2}$ and $1d_{3/2}$ shells in ^{40}Ca (b). Experimental data are from Refs. [6,7]. Solid lines are the results of DWBA+DWIA calculations with the *cc*1 operator, scaled by the spectroscopic factors in the third column of Table II. The dotted line in (b) corresponds to the result with PWBA+DWIA with the *cc*1 operator. The dashed line in (b) corresponds to the result with the *cc*2 operator.

ing and corresponds to a different $3s_{1/2}$ relativistic wave function leading to a smaller spectroscopic factor. Nevertheless, it is important to remark that all the results of the relativistic calculations for ^{208}Pb are in agreement within 10% and are compatible with theoretical predictions [1–3], while the previous results from the nonrelativistic analyses are clearly too low. These too small spectroscopic factors in the nonrelativistic analyses of Refs. [6,7] result from too much focusing of the electron waves and too little absorption of the outgoing proton wave, compared to the relativistic analyses, as was discussed in detail in the previous section (see Table I and Fig. 4).

It should be stressed here that in our analysis the determination of the spectroscopic factors has no free parameters. All of the parameters entering in the relativistic potentials were obtained from independent considerations [20,18]. Taking this into account it is remarkable the good quality of the fits to the experimental data seen in Fig. 5(a) for the two shells in ^{208}Pb. To have a measure for the quality of the fit, we consider the parameter Q defined as the χ^2 value divided by the degrees of freedom (number of data involved minus one) in the determination of the spectroscopic factor. In our cases $Q < 3$ corresponds to a good quality of the fit while $Q > 5$ corresponds to a poor fit. The Q values obtained for ^{208}Pb are $Q < 3$ for both shells $(3s_{1/2}, 2d_{3/2})$ and for both types of current operators. Our results in Fig. 5(a) correspond to the calculations with the *cc*1 operator, using the spectroscopic factors in column three of Table II. Similar results are obtained using the *cc*2 operator and the spectroscopic factors of column four in Table II.

In the case of ^{40}Ca the focusing effect is negligible and the only noticeable effect of electron Coulomb distortion is a shift in P_m. This is illustrated in Fig. 5(b) for the $2s_{1/2}$ orbital where we plot the DWBA result (solid line) and the result in PWBA with $q_{\rm eff}$ (dotted line), both using the *cc*1 operator and the same spectroscopic factor ($S = 0.44$, see Table II). The effective momentum corresponds to $f_c = 1.35$ in Eq. (3.2). As seen in the figure there is no significant difference between the results in DWBA and in PWBA with $q_{\rm eff}$. Although not shown in the figure, the same is true with regard to DWBA and PWBA calculations for the $1d_{3/2}$ orbital in ^{40}Ca.

As seen in Fig. 5(b) the agreement between our theoretical results for the $2s_{1/2}$ and for the $1d_{3/2}$ shells in ^{40}Ca with the *cc*1 current operator is not as good as that obtained for the shells in ^{208}Pb. If we use instead the *cc*2 operator, the agreement is not improved for the $2s_{1/2}$ shell, but it improves considerably for the $1d_{3/2}$ shell. This is seen in Fig. 5(b) where we show our results for the $1d_{3/2}$ shell with the *cc*1 and the *cc*2 operators by solid and dashed lines, respectively. For the case of the $2s_{1/2}$ shell the Q value is larger than 7 in all cases, showing the poor quality of the fit. For the $1d_{3/2}$ shell the Q value is almost 5 in the case of the *cc*1 operator and is less than 2 in the case of the *cc*2 operator.

It is important to realize that all the cases where our spectroscopic factors in columns three and four of Table II are low correspond to situations in which the shape of the theoretical curve does not match well the trend in the experimental data and the Q values are large, i.e., the fits are poor. This is particularly the case for the $2s_{1/2}$ shell in ^{40}Ca, where our spectroscopic factor is as low as that obtained in the nonrelativistic analysis of Ref. [7]. For the shell $1d_{3/2}$ in ^{40}Ca, where the fit with the *cc*2 operator is very good, we get a spectroscopic factor $S = 0.76$, similar to that found in ^{208}Pb, and larger than the one obtained in the nonrelativistic analysis [7].

In the case of ^{40}Ca the comparison of our results with those of Ref. [12] is not as meaningful as in the case of ^{208}Pb for the two following reasons: (i) the bound nucleon wave functions used in Ref. [12] were different [28] than the standard TIMORA solutions used here and (ii) the spectroscopic factors in Ref. [12] were derived by visual fitting. However it is interesting to see that the result of Jin *et al.* [12] agrees with the one we obtain for the $1d_{3/2}$ shell with the *cc*2 operator, where we consider our deduced spectroscopic factor to be reliable.

IV. CONCLUDING REMARKS

We have analyzed the quasielastic $(e, e'p)$ reaction within a fully relativistic formalism treating the Coulomb distortion of the electrons in an exact way. This analysis is expected to yield more reliable spectroscopic factors than previous analyses where the electron Coulomb distortion was not fully taken into account [10,11].

We present results for reduced cross sections as functions of the missing momentum (P_m), corresponding to proton knock-out from the outermost shells in ^{40}Ca and in ^{208}Pb. We study the effects purely due to electron Coulomb distortion as well as the effects due to the relativistic treatment of the initial (bound) and final (distorted) nucleon wave functions. We also study the effects of using different nucleon current operators.

In parallel kinematics, Coulomb distortion produces two effects: (i) displacement of the cross section toward higher P_m values that can be simulated by the use of an effective momentum transfer $q_{\rm eff}$ in PWBA and (ii) fo-

cusing that shows up mainly in the maxima and minima of the reduced cross section.

The focusing effect plays an important role in the determination of the spectroscopic factors in ^{208}Pb. In ^{40}Ca the focusing effect is much smaller than in ^{208}Pb and has no influence in the extraction of spectroscopic factors, but the displacement effect is still sizable. Exact DWBA calculations are worthwhile even in medium nuclei like ^{40}Ca in order to determine the precise magnitude of this displacement and to avoid introducing additional parameters.

In perpendicular kinematics, we do not find displacement in P_m but there is an apparent increase of focusing (or antifocusing) at $P_m \sim 0$, caused by the effective momentum transfer.

We find that the main difference between the results obtained with our relativistic treatment of the nuclear vertex and with the usual nonrelativistic treatment [6,7] is due to the fact that the relativistic optical potential [20] produces more absorption in the $(e,e'p)$ reaction. This gives rise to higher spectroscopic factors in much better agreement with theoretical predictions [1–3]. In our view this is a strong point in favor of the relativistic S-V models that are able to account for both elastic proton-nucleus and $(e,e'p)$ data simultaneously and confirms the fact that the relativistic phenomenology is in general superior to the usual nonrelativistic phenomenology in covering a large variety of experimental information on proton-nucleus scattering and particularly in what concerns spin rotation functions (see Ref. [29] and references therein).

We also find that the off-shell electron-proton cross section is less sensitive to the choice of the nucleon current operators when using free Dirac spinors [21,22] than when using bound Dirac spinors. Thus, one should be cautious when estimating the uncertainty associated with the current operator from results based only on free spinors. Actually, further work is needed to clarify the situation with regard to the best choice of the nucleon current operator in the fully relativistic treatment of the $(e,e'p)$ reaction.

The spectroscopic factors have been obtained by scaling to experimental data the calculated reduced cross sections without introducing any free parameter. For the $3s_{1/2}$ and $2d_{3/2}$ shells in ^{208}Pb we find spectroscopic factors between 0.65 and 0.73 depending on the shell and on the nucleon current operator. High quality fits to the experimental reduced cross sections are obtained in all the cases. These spectroscopic factors are in agreement with theoretical predictions and with the results obtained for the $3s_{1/2}$ shell in ^{208}Pb by Jin *et al.* [12] from a fully relativistic analysis analogous to the one carried out here. They are considerably larger than the spectroscopic factors obtained from the nonrelativistic analyses [6].

For ^{40}Ca we only obtain a high quality fit to the data for the $1d_{3/2}$ shell when using the $cc2$ operator. In this case the value of the extracted spectroscopic factor is 0.76, similar to those obtained in ^{208}Pb. For the $2s_{1/2}$ shell the quality of the fit is very poor with both $cc1$ and $cc2$ operators and, therefore, we cannot consider the deduced spectroscopic factors as being reliable. In our view, if the shape of the cross section is not well reproduced, the derived spectroscopic factor is not meaningful. For this particular orbital the wave function obtained from the TIMORA code used here does not reproduce the experimentally observed shape of the reduced cross section. In comparing with the results by Jin *et al.* [12] for these two orbitals in ^{40}Ca, one should keep in mind that there are two main differences between their calculations and ours; (i) the results reported in Ref. [12] were obtained using a phenomenological potential fitted to reproduce single-particle properties in ^{40}Ca [28]; (ii) their spectroscopic factors are obtained by visual fit and no quality of the fit is reported to compare with ours. Nevertheless, in the case of the shell $1d_{3/2}$ with the $cc2$ operator, where the quality of our fit is good, our spectroscopic factor agrees with that of Ref. [12].

In this work we made no attempt to fit to experiment the rms radii and binding energies of the orbitals. Thus, the fact that we get high quality fits for all the orbitals studied, except the $2s_{1/2}$ in ^{40}Ca, can be considered as a success of the relativistic analysis. It would be interesting to explore whether more elaborate relativistic S-V models, including nonlinear terms, may produce results in better agreement with experimental data on reduced cross sections for the $2s_{1/2}$ shell in ^{40}Ca.

ACKNOWLEDGMENTS

We are grateful to J. McDermott for providing us with his HCA code and for useful discussions and to L. Lapikás and G. van der Steenhoven for communication of experimental data collected at NIKHEF-K. One of us (J.M.U.) also thanks Y. Jin for helpful comments. This work has been partially supported by DGICYT (Spain) under Contract No. 92/0021-C02-01.

[1] C. Mahaux and R. Sartor, Adv. Nucl. Phys. **20**, 1 (1991).
[2] Z.Y. Ma and J. Wambach, Phys. Lett. B **256**, 1 (1991).
[3] V.R. Pandharipande, C.N. Papanicolas, and J. Wambach, Phys. Rev. Lett. **53**, 1133 (1984).
[4] J.M. Cavedon *et al.*, Phys. Rev. Lett. **49**, 978 (1982); E.N.M. Quint *et al.*, *ibid.* **57**, 186 (1986); E.N.M. Quint *et al.*, *ibid.* **58**, 1088 (1987).
[5] I. Sick and P.K.A. de Witt Huberts, Comments Nucl. Part. Phys. **20**, 177 (1991).
[6] E.N.M. Quint, Ph.D. thesis, University of Amsterdam, 1988.
[7] G.J. Kramer, Phys. Lett. B **227**, 199 (1989); Ph.D. thesis, University of Amsterdam, 1990.
[8] P.K.A. de Witt Huberts, J. Phys. G **16**, 507 (1990).
[9] S. Frullani and J. Mougey, Adv. Nucl. Phys. **14**, 1 (1985).
[10] C. Giusti and F. Pacati, Nucl. Phys. **A473**, 717 (1987); **A485**, 461 (1988); M. Traini, Phys. Lett. B **213**, 1 (1988).

[11] J.P. McDermott, Phys. Rev. Lett. **65**, 1991 (1990).
[12] Y. Jin, D.S. Onley, and L.E. Wright, Phys. Rev. C **45**, 1311 (1992).
[13] J.M. Udías, Ph.D. thesis, Universidad Autónoma de Madrid, 1993.
[14] J.D. Björken and S.D. Drell, *Relativistic Quantum Mechanics* (McGraw-Hill, New York, 1964).
[15] H. Uberall, *Electron Scattering from Complex Nuclei* (Academic, New York, 1971); M.E. Rose, *Relativistic Electron Theory* (Wiley, New York, 1961).
[16] D.R. Yennie, R.N. Wilson, and D.G. Ravenhall, Phys. Rev. **95**, 500 (1954).
[17] H. de Vries, C.W. de Jager, and C. de Vries, At. Data Nucl. Data Tables **36**, 495 (1987).
[18] C.J. Horowitz and B.D. Serot, Nucl. Phys. **A368**, 503 (1981); Phys. Lett. **86B**, 146 (1979).
[19] C.J. Horowitz, D.P. Murdock, and B.D. Serot, *Computational Nuclear Physics* (Springer-Verlag, Berlin, 1991).
[20] S. Hama, B.C. Clark, E.D. Cooper, H.S. Sherif, and R.L. Mercer, Phys. Rev. C **41**, 2737 (1990); S. Hama, E.D. Cooper, B.C. Clark, and R.L. Mercer, in *Global Dirac Phenomenology for Proton–Nucleus Elastic Scattering*, Ohio State University report, 1992.
[21] T. de Forest, Jr., Nucl. Phys. **A392**, 232 (1983).
[22] J.A. Caballero, T.W. Donnelly, and G.I. Poulis, Nucl. Phys. **A555**, 709 (1993).
[23] J.P. McDermott, private communication.
[24] K.V. McVoy and L. van Hove, Phys. Rev. **125**, 1034 (1962).
[25] H.P. Blok, L.R. Kouw, J.W.A. den Herder, L. Lapikás, and P.K.A. de Witt Huberts, Phys. Lett. B **198**, 4 (1987).
[26] P. Schwandt, H.O. Meyer, W.W. Jacobs, A.D. Bacher, S.E. Vigdor, M.D. Kaitchuck, and T.R. Donoghue, Phys. Rev. C **26**, 55 (1982).
[27] S. Boffi, C. Giusti, F.D. Pacati, and F. Cannata, Nuovo Cimento **98**, 291 (1987).
[28] Y. Jin, Ph.D. thesis, Ohio University, 1991.
[29] B.C. Clark, R.L. Mercer, and P. Schwandt, Phys. Lett. **122B**, 211 (1983); H. Feshbach, *Theoretical Nuclear Physics* (Wiley, New York, 1992).